Increased Wave Break During Ventricular Fibrillation in the Epicardial Border Zone of Hearts With Healed Myocardial Infarction

Toshihiko Ohara, MD; Keiko Ohara, MD; Ji-Min Cao, MD; Moon-Hyoung Lee, MD; Michael C. Fishbein, MD; William J. Mandel, MD; Peng-Sheng Chen, MD; Hrayr S. Karagueuzian, PhD

Background—The action potential duration (APD) restitution hypothesis of wave break during ventricular fibrillation (VF) in the epicardial border zone (EBZ) of hearts with chronic myocardial infarction is unknown.

Methods and Results—VF was induced by rapid pacing, and the EBZ with the two adjoining sites (right ventricle and lateral left ventricle) were sequentially mapped in random order in 7 open-chest anesthetized dogs 6 to 8 weeks after left anterior descending artery occlusion and in 4 control dogs. At each site, 3 seconds of VF was mapped with 477 bipolar electrodes 1.6 mm apart. The number of wave fronts and approximate entropy were significantly ($P<0.01$) higher in the EBZ than all other sites in both groups independent of the rate of invasion of new wave fronts and epicardial breakthroughs. The higher wavelet density in the EBZ was caused by increased ($P<0.01$) incidence of spontaneous wave breaks. There was no difference between the two groups in either reentry period (80 episodes) or VF cycle length. Reentry in the EBZ had a smaller core perimeter, slower rotational speed, and a small or no excitable gap ($P<0.01$), often causing termination after one rotation. The dynamic monophasic action potential duration restitution curve in the EBZ had longer ($P<0.01$) diastolic intervals, over which the slope was >1. Connexin43-positive staining was significantly ($P<0.01$) and selectively reduced in the EBZ.

Conclusions—A selective increase in wave break and alteration of reentry occur in the EBZ during VF in hearts with healed myocardial infarction. Increased wave break in the EBZ is compatible with the action potential duration restitution hypothesis. **(*Circulation*. 2001;103:1465-1472.)**

Key Words: myocardial infarction ■ fibrillation ■ action potentials ■ waves

Ventricular fibrillation (VF) in normal ventricles may be maintained by either a generalized wave break throughout both ventricles[1–3] or by breakups of the wave fronts emanating at a fast rate from a presumed single stable reentrant source.[4] In either dynamic scenario, wave breaks provide a continuous source of rapid and irregular reentrant and/or nonreentrant activations ("fibrillatory conduction") that sustains the VF.[1–4] Wave break is caused by a conduction block at a given site of the wave front that may be caused by an increase in the range of diastolic intervals (DI), over which the action potential duration (APD) restitution slope remains >1.[5–7] However, at present, it is unknown if the APD restitution also predicts vulnerability to wave break during VF in the epicardial border zone (EBZ) with altered gap junctional (Connexin [Cx]43) couplings.[8–10] It is also unclear how the EBZ influences reentry characteristics. For example, in normal cardiac muscle, the reentry period shortens as the core size shrinks.[2,11,12] Whether such a relation also exists in the EBZ with altered excitability[13] and anatomy[8–10] remains undefined. Kadish et al[14] have shown altered (vector) activation pattern during VF in hearts with healed myocardial infarction (MI); however, the role of APD restitution in wave break and reentry characteristics in the EBZ during VF were not evaluated in this study. We hypothesized that the electrical and anatomic changes (remodeling) in the EBZ promote wave break and alter the characteristics of the reentrant wave front during VF in hearts with chronic (healed) MI. The purpose of this study was to test these two hypotheses.

Methods

Surgical Preparation

The research protocol was approved by the Institutional Animal Care and Use Committee of Cedars-Sinai Medical Center and followed the guidelines of the American Heart Association. Seven mongrel dogs of either sex weighing 23 to 28 kg were anesthetized with intravenous sodium pentobarbital (35 mg/kg), and MI was induced

Received August 16, 2000; revision received September 15, 2000; accepted September 19, 2000.

From the Division of Cardiology, Cedars-Sinai Research Institute, the Departments of Medicine and Pathology, UCLA School of Medicine, Los Angeles, Calif.

Correspondence to Hrayr S. Karagueuzian, PhD, Cedars-Sinai Medical Center, Davis Research Bldg, Room 6066, 8700 Beverly Blvd, Los Angeles, CA 90048. E-mail karagueuzian@csmc.edu

Circulation **is available at http://www.circulationaha.org**

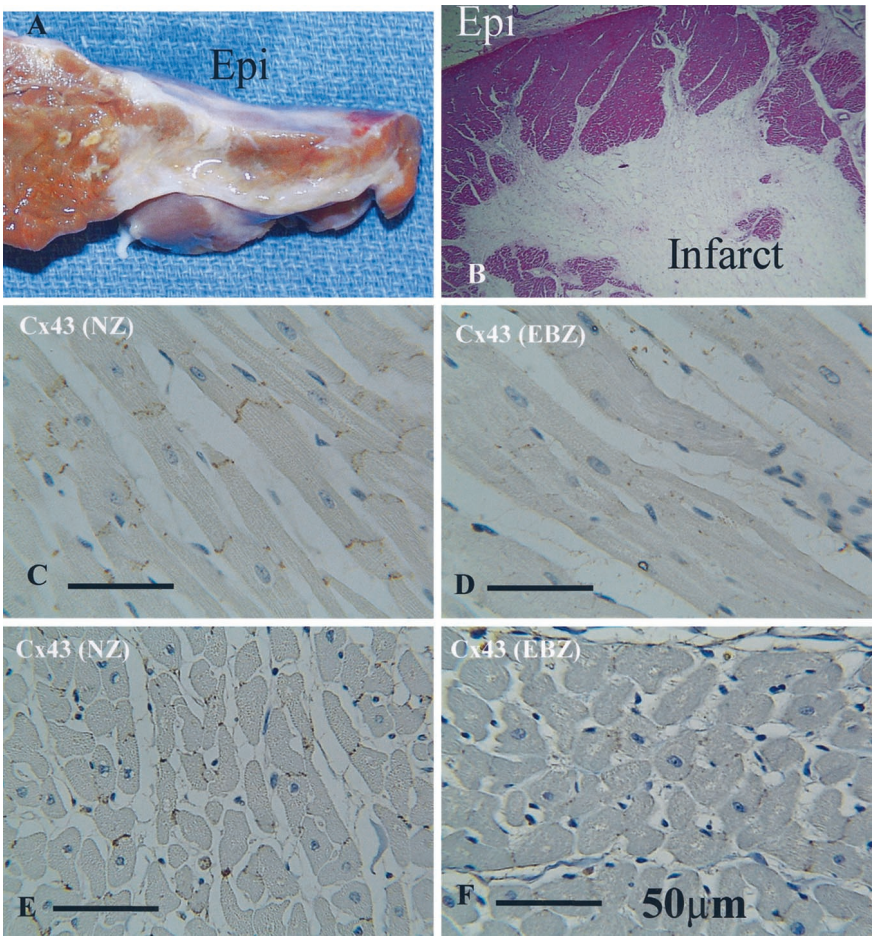

Figure 1. Histopathological and immunostaining with Cx43. A, Gross anatomy of transmural section of infarcted LV (8 weeks after LAD occlusion). Whitish areas are scar tissue. B, Hematoxylin and eosin microscopic section showing EBZ (Epi) over deeper scar tissue (infarct). C and E, Longitudinally and transversely oriented normal myocardium showing numerous Cx43 stains. D and F show similar sections in EBZ, with reduced Cx43 staining. Bar is 50 μm.

by permanent left anterior descending coronary artery (LAD) occlusion distal to the first diagonal branch.[15] Dogs were then restudied 6 to 8 weeks later in the open-chest state.[1,16,17] Four dogs with no LAD occlusion served as control.

Monophasic Action Potential Restitution

Dynamic monophasic APD restitution curves were constructed in all mapped regions of MI and the control groups.[12,18]

Computerized Mapping During VF

VF was induced by rapid pacing as described previously.[19] Three seconds after the onset of each VF episode, 3 seconds of data were acquired with a 3.2×3.8-cm plaque containing 477 bipolar electrodes 1.6 mm apart.[20] The VF was then converted by electrical shocks of 15 J with internal paddles. After 5 to 10 minutes of recovery, VF was reinduced and activation mapped from another site. The order of mapping sites was randomized. Activation pattern and wave front number were determined by dynamic visualization.[3,20] The VF cycle length (CL) was measured on each channel over the entire 3 seconds of VF in each dog and was averaged. Typically, in each dog, >400 channels were of acceptable quality for VF CL calculations, for a total of >9000 beats in each dog (20 to 22 cycles over 400 channels).[1,16,17] Data are presented as mean VF CL in each group.

Measurement of Reentry Core Perimeter

Once a reentrant wave front was detected, the inner edge of the core was traced for one complete rotation, and core perimeter and average conduction velocity (CV) around the core were measured.[1,12,16,21] The CV of nonreentrant wave fronts, along and across the fiber, were also measured during VF and during regular pacing by dividing conduction time over distance in a region of consecutively activated adjacent electrodes.[22] The effective refractory period (ERP) during VF was estimated by perpendicular wave-wave interaction as described before[1,12] and during regular pacing at 400-ms CL by the extrastimulus method.[2,11,12]

Approximate Entropy

Three seconds of a bipolar electrogram sampled at 1 kHz (3000 points) was used for approximate entropy (ApEn) calculations (temporal complexity), as described previously.[23]

Histological Studies

Ventricles were sectioned from apex to base in 1- to 1.5-cm-thick transverse slices, and Cx43 was stained with antibodies by the ABC method (Santa Cruz Biotechnology Inc).[24] The percentage of positive Cx43 staining was calculated in ≥20 different fields in each section by Image-Pro software (Media-Cybernetics). Infarct size was determined from hematoxylin and eosin transverse sections by planimetry.[15,25]

Statistical Analysis

All statistical analyses were performed with GB-STAT,[26] Student's *t* tests for single comparison, and ANOVA for multiple comparisons with Newman-Keuls post hoc analyses. The null hypothesis was rejected at a value of $P \leq 0.05$. Results are expressed as mean±SD.

Results

Infarct Size and Location

In all dogs LAD occlusion caused MI in the anteroapical site sparing 30 to 100 epicardial cell layers over the infarct (EBZ) (Figure 1). The mean infarct size was 19±3% of the total (225±15 g) left ventricular (LV) mass.

TABLE 1. Wave Front and Electrophysiological Properties in Dogs With Chronic Myocardial Infarction

	RV	EBZ	Lateral LV	*P*
Threshold, mA	0.57±0.26	0.81±0.30	0.58±0.22	*§
ERP, ms	168.2±11.3	188.0±18.0	168.0±16.3	*§
CL during VF, ms	134.1±18.0	135.2±17.3	136.0±18.9	NS
Wavelet n/10 ms	3.08±0.27	4.29±0.24	2.98±0.29	†‖
ApEn	0.212±0.010	0.251±0.024	0.184±0.013	*‡¶
CV along, cm/s	55.5±14.4	35.3±6.4	57.4±14.7	†‖
CV across, cm/s	35.7±6.2	28.7±5.6	36.3±5.5	†§
Anisotropic ratio	1.66±0.56	1.19±0.24	1.68±0.55	†‖
Reentry episodes	20	17	15	
Core perimeter, cm	2.65±0.36	1.95±0.26	3.06±0.26	†‖**
Reentry period, ms	100.5±9.8	100.3±10.4	102.8±12.6	NS
Reentry CV, cm/s	25.9±3.0	19.2±2.7	29.5±2.9	†‖**
Max slope	2.27±0.5	3.61±0.34	1.36±0.14	†§¶
DI >1, ms	16.0±0.9	23.2±1.3	12.8±1.9	*‡¶

ERP was determined during regular pacing at 400-ms CL by the extrastimulus method; wavelet n/10 ms is the number of independent wave fronts in the mapped region counted in 10-ms increments over a 3-second VF interval (300 frames).

EBZ vs lateral LV, *$P<0.01$, †$P<0.001$.

EBZ vs RV, ‡$P<0.05$, §$P<0.01$, ‖$P<0.001$.

RV vs lateral LV, ¶$P<0.05$, **$P<0.001$.

Number of Wave Fronts During VF

During regular pacing, no conduction block occurred over the entire EBZ in each dog, indicating that the observed blocks during the VF were functional in nature. The ERP during the VF, estimated by the method of perpendicular wave-wave interaction,[1] was significantly ($P<0.01$) longer in the EBZ than in the anterior LV of control dogs (115±13 ms versus 87±11 ms). Significantly fewer ($P<0.001$) epicardial breakthroughs occurred in the EBZ than at all other sites in both groups (Figure 2 and 3). Epicardial breakthroughs occurred 6.75±0.9/s in the normal zones of both groups (11% of all wave front activity), whereas in the EBZ, the breakthroughs occurred only 1.72±0.75/s, accounting to 0.73±0.14% of overall wave front activity. The rate of invasion of new wave fronts from adjoining lateral regions was not significantly different in the EBZ compared with normal non-MI anterior LV (48.3±6.6/s versus 51±5.3/s, P=NS). The average num-

TABLE 2. Wave Front and Electrophysiological Properties in Dogs With No Myocardial Infarction

	RV	Anterior LV	Lateral LV	*P*
Threshold, mA	0.48±0.12	0.52±0.17	0.50±0.14	NS
ERP, ms	169.5±6.5	171.0±4.1	168.0±16.3	NS
CL during VF, ms	131.4±3.3	134.1±4.1	131.3±4.3	NS
Wavelet n/10 ms	2.96±0.05	3.03±0.06	2.98±0.05	NS
ApEn	0.189±0.018	0.184±0.012	0.186±0.026	NS
CV along, cm/s	53.5±14.0	52.7±12.0	53.0±13.0	NS
CV across, cm/s	36.9±5.5	38.6±5.9	36.0±6.0	NS
Anisotropic ratio	1.50±0.44	1.50±0.37	1.52±0.44	NS
Reentry episodes	10	10	8	
Core perimeter, cm	3.10±0.44	3.12±0.40	3.00±0.40	NS
Reentry period, ms	100.0±12.2	104.6±7.9	101.3±7.4	NS
Reentry CV, cm/s	30.1±2.4	30.3±3.8	29.1±2.5	NS
Max slope	1.53±0.13	1.58±0.17	1.45±0.13	NS
DI >1, ms	13.7±1.5	14.3±1.5	13.7±2.1	NS

ERP was determined during regular pacing at 400-ms CL by the extrastimulus method; wavelet n/10 ms is the number of independent wave fronts in the mapped region counted in 10-ms increments over a 3-second VF interval (300 frames).

RV vs anterior LV; RV vs lateral LV; anterior LV vs lateral LV.

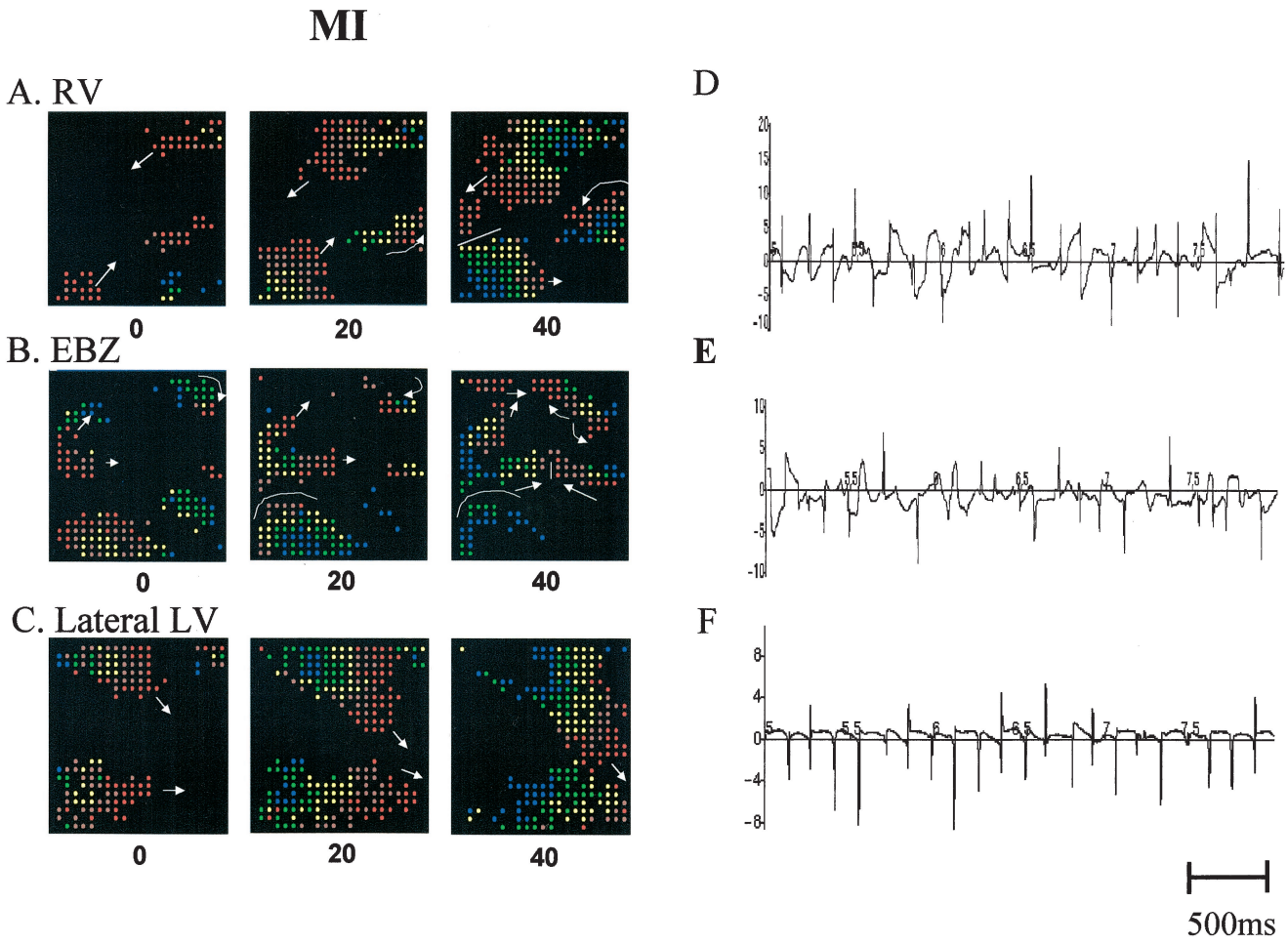

Figure 2. Selected snapshots obtained sequentially from 3 different sites in a dog 8 weeks after LAD occlusion. A, Plaque in RV; at time 0, two wave fronts enter mapped area (arrow), with third breakthrough wave front in middle right of plaque. These fronts propagate to edges of plaque without breakups. B, In EBZ, total of 4 wave fronts. Two wave fronts entering plaque (arrows) undergo breakups with conduction blocks occurring in middle of both fronts. Third (bottom) and fourth (middle right) wave fronts undergo block (bottom) and collision, with subsequent annihilation in both cases. C, In normal noninfarcted LV, 3 wave fronts (time 0) propagate downward (arrows) and coalesce together before exiting plaque. Most recent activated site is shown in red, then pink, then yellow, then green, and finally, blue. Persistence of each color is 10 ms. Selected bipolar electrograms (D, E, and F) are shown next to each panel with similar CLs.

ber of wavelets in the mapped region was significantly ($P<0.001$) higher in the EBZ than all other sites in both groups. (Tables 1 and 2). The higher number of wave fronts in the EBZ compared with other sites resulted from the more frequent spontaneous breakups. Breakup occurred when a wave front encountered refractory tissue from a previous activation (Figure 2B and Figure 3C). The mean number of wave breaks (counted over 3 seconds at 10-ms intervals) was significantly ($P<0.001$) higher in the EBZ than in the left anterior wall in the non-MI group (19.3 ± 2.5/s versus 8 ± 1.4/s). To ensure reproducibility of the observed results, wave front number and ApEn (see below) determinations were repeated by the same investigator and by a second investigator blinded to the origin of the data (a total of 33 episodes of VF in 7 dogs). A linear regression analysis that was run between the intraobserver and interobserver measurement outcomes yielded a correlation coefficient of 0.97 and 0.96, respectively, for both measurements.

Wave Front Collisions

In addition to head-and-tail interactions, two wave fronts could collide head on or roughly perpendicular to each other. The consequences of head-head wave front collisions were different in the EBZ compared with all other sites in both groups. Collision in the EBZ (5 ± 1/s) resulted in wave front annihilation in 71% of the episodes (Figure 2B) and survival in 29%, with subsequent propagation of the wave front in a direction perpendicular to the direction of collision. In the normal anterior LV however, collision (7 ± 1/s, $P=$NS, compared with EBZ) caused annihilation in 54% of the episodes and survival in 46% of episodes with propagation in a direction perpendicular to the direction of collision (Figure 3B). The differences in the outcome of the head-on collisions (annihilation and survival) were significantly ($P<0.01$) different in the EBZ compared with similar LV anterior site in the non-MI control group.

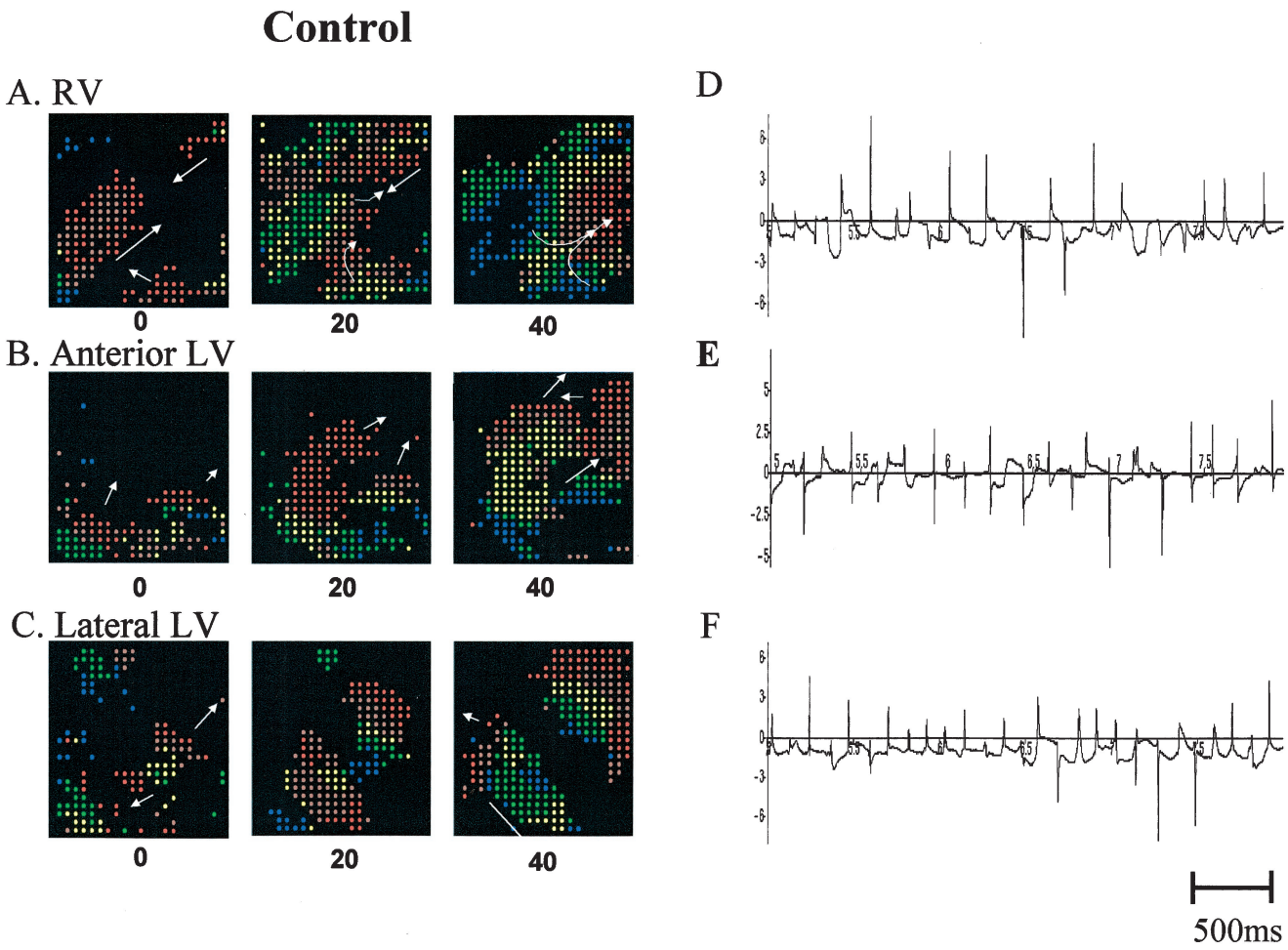

Figure 3. Selected snapshots obtained sequentially from 3 different sites in a dog with no LAD occlusion. All panels were obtained from similar sites as in Figure 2. At all sites, note presence of relatively large wave fronts (arrows) that either collide with each other (A), join with each other (B), or propagate in different directions (C) to exit from plaque site. Selected electrograms from each site are shown next to panels (D, E, and F). Color code as in Figure 2.

The VF CL was not different at all three sites in both groups; however, the ApEn was significantly ($P<0.05$) higher in the EBZ than all other sites in both groups (Tables 1 and 2).

Reentrant Wave Front Characteristics During VF

A total of 80 episodes of complete reentrant activations were captured during VF in both groups (Figure 4). The core perimeter of the reentry was significantly ($P<0.01$) shorter and had slower speed in the EBZ compared with all other sites in both groups ($P<0.05$; Tables 1 and 2 and Figure 4). The core of the reentry in the EBZ became roughly circular instead of elliptic, which was seen at all other sites in both groups (Figure 4). The similar reentry period at all sites narrowed or closed the excitable gap at the EBZ because of the longer ERP in the EBZ during VF. The smaller excitable gap during reentry in the EBZ caused the reentry to terminate after only 1 rotation (4 episodes) or after an incomplete "reentry" (10 episodes). Two to 3 consecutive rotations during reentry were seen in a total of 11 episodes at normal sites in both groups.

CV of Nonreentrant Wave Fronts During VF

A total of 179 CV measurements of nonreentrant wave fronts were made during VF in both groups. At all sites, the CV was significantly slower in the EBZ both along and across the fiber orientation (Tables 1 and 2). Although the directional differences in CV were decreased in the EBZ compared with normal, CV still remained significantly ($P<0.05$) faster along than across the fiber orientation in the EBZ.

Dynamic APD Restitution Relation

The maximum slope and the range of DIs within which the slope of the APD restitution curve remained >1 were significantly higher in the EBZ than all other sites in both groups (Table 1 and Figure 5).

Cx43 Distribution

Immunostaining showed a selective and significant ($P<0.001$) reduction of Cx43 distribution in the EBZ. Cx43 was reduced both in the end-to-end and side-to-side locations (Figure 1). Cx43 was $0.77\pm0.17\%$ of the total tissue area in the normal zones in both groups versus $0.17\pm0.06\%$ in the EBZ ($P<0.001$) (Figure 1). At distances 3 to 5 mm away from the EBZ, however, staining of Cx43 increased and became normal 1 cm away from the EBZ. These findings are consistent with the earlier electron micrographs of gap junctions[9] and connexin staining[10] in hearts with healed MI.

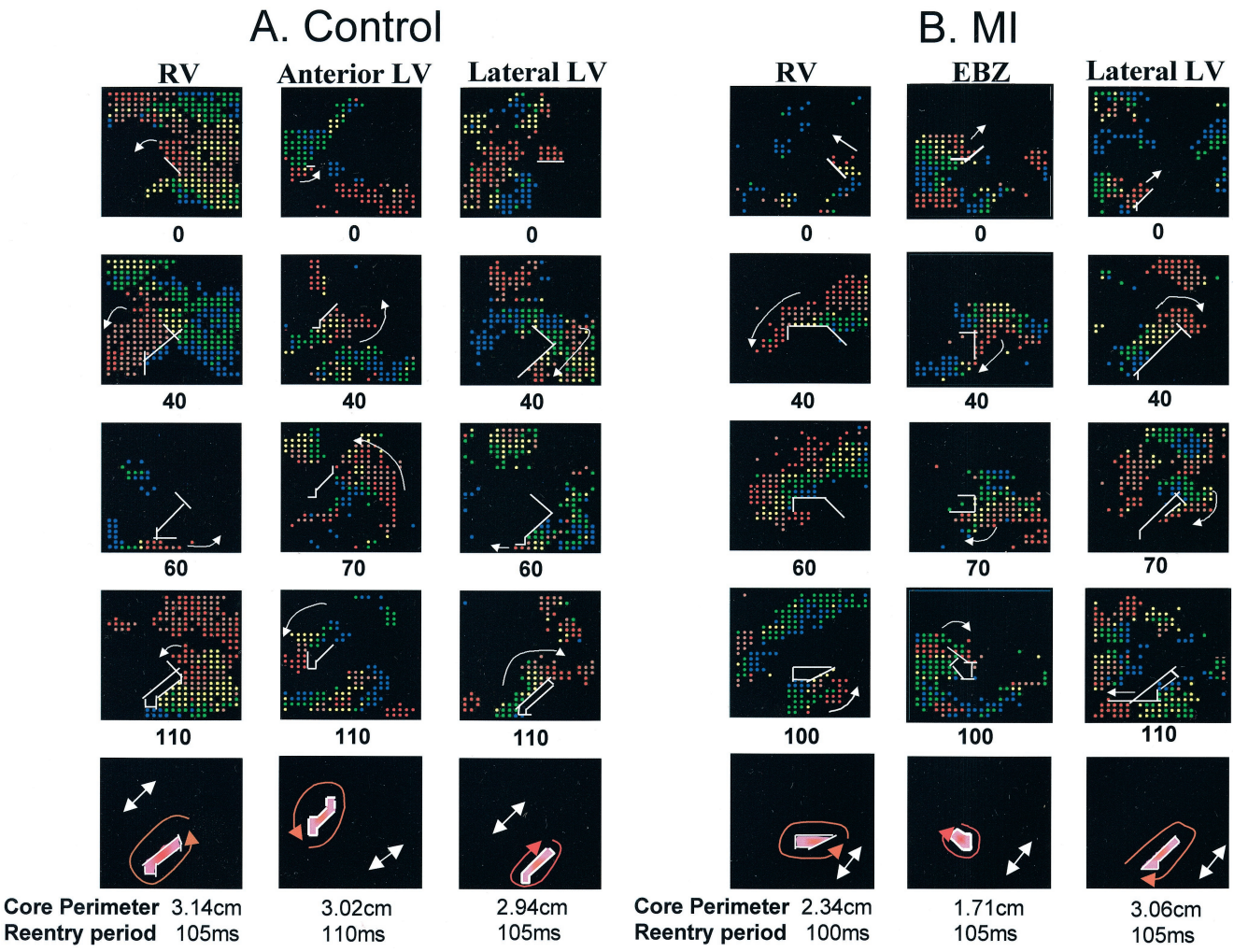

Figure 4. Reentrant wave fronts during VF at different sites in both groups. In each row, selected snapshots are shown during formation of reentrant wave front (white arrows). Note smaller and relatively circular core in EBZ and slower CV compared with all other sites. Lowest frames in each panel show location, size, and shape of central core of reentry, with direction of rotation pointed by circular red arrow. White double-headed arrow in each frame points to long axis of myocardial fiber orientation. Abbreviations and color code as in Figure 2.

Discussion

Major Findings

The increased incidence of spontaneous wave break in the EBZ during VF compared with adjoining normal sites and to comparable sites in control non-MI dogs constitutes a major finding in the present study. A second major finding of this study is the loss of the normal relation in the EBZ between ERP and reentry period.[2,11,12] Although in the normal ventricle lengthening of the ERP lengthens the period of reentry, the longer ERP in the EBZ, however, failed to lengthen the reentry period. Finally, the slower CV in the Cx43-deficient EBZ appeared to prevent faster activation during VF (CL shortening) that might have been caused by the denser EBZ wavelets.

Why Regional Differences in Wave Front Dynamics?

The difference of the APD restitution properties in the EBZ compared with adjoining sites might provide a basis for the observed regional differences in wave front dynamics. Simulation studies showed that an increase in the range of DIs of the APD restitution curve over which the slope is >1 promotes wave front breakups.[6] The dynamic APD restitution relation, which closely resembles the restitution during VF,[12] showed that the EBZ cells manifest higher maximum slopes and a significantly wider range of DIs over which the slope remained >1. Although the restitution hypothesis is compatible with the higher incidence of wave break in the EBZ, additional mechanisms of wave break may also be operative in the EBZ. For example, increased ERP and partial cellular uncoupling (decreased Cx43) might increase vulnerability to wave break.[8] As the number of wavelets in the EBZ increased, so did the complexity of VF, as indicated by the increase in the ApEn. This finding is consistent with previous reports on isolated porcine right ventricle (RV).[3] Whereas complexity and wave front density increased, the VF CL however did not change, an effect probably caused by the severe CV slowing in the EBZ that offsets the potential of more frequent activations by the denser wave fronts.

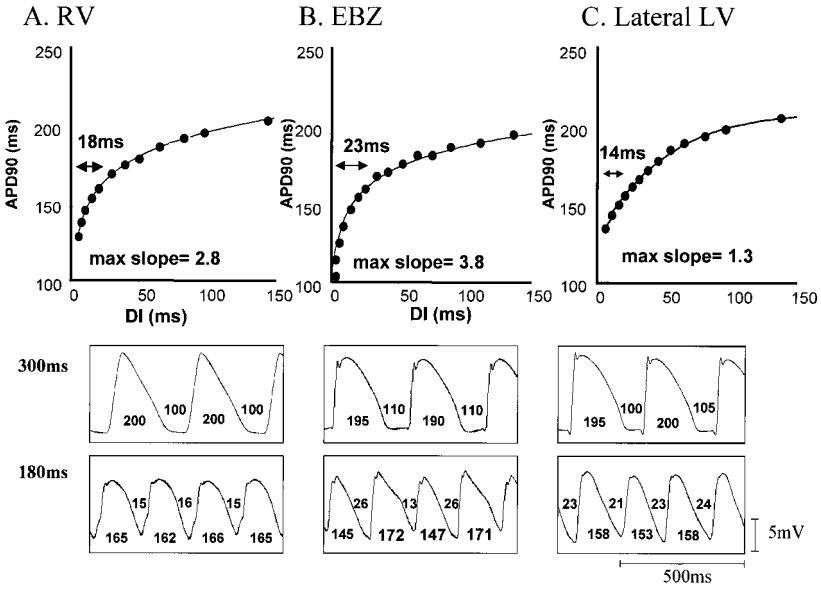

Figure 5. Regional difference of DI-APD_{90} restitution relations in a dog 6 weeks after LAD occlusion. Upper panels: A is RV, B is EBZ, and C is lateral LV. Double-headed arrows next to each curve indicate DI intervals, over which slope is >1. Lower panels show dynamic MAP recordings during 300-ms and 180-ms pacing cycle lengths.

Dynamics of Reentry in EBZ

Severe conduction slowing along and across the fiber in the Cx43-deficent EBZ changed the elliptical shape of the reentry core to a more or less circular one. Such a change in the shape of the reentry core may be caused by a significant ($P<0.01$) decrease in the anisotropic ratio from 1.6 ± 0.5 in normal sites in both groups to 1.19 ± 0.24 in the EBZ (Table 1). The slowing of the CV in the EBZ during reentry, however, did not prolong the period of the reentry because of a concomitant reduction in the core size of the reentry (scaling). Although the mechanism of core shrinking in the EBZ remains to be defined, we speculate that reduced gap-junctional Cx43 might promote such an effect because the longer ERP in the EBZ would have increased and not decreased the core size.[2,11,12] More work is needed to determine the mechanism(s) by which the reentry core size versus reentry period relation becomes altered in the EBZ.

Clinical Relevance

Although speculative, it is possible that increased susceptibility to wave break observed during VF in the EBZ might be related to increased vulnerability to VF in patients with chronic MI, because increased propensity to wave break might lead to VF.[5,6] This speculation, however, needs mapping data on human ventricles with chronic MI to ascertain the wave break hypothesis of VF in humans.

Limitations of the Study

Because recordings from different sites during a VF episode were not simultaneous, it could be argued that the observed regional differences in wave front dynamics might be caused by differences in different VF episodes. However, the presence of similar wave front dynamics, reentry morphology, and CV at a given site on repeat VF episodes (data not shown) and randomized acquisition of data from different sites refutes this possibility. It may be argued that our maps are 2D and not 3D, raising doubt on the interpretation of the EBZ maps. However, the EBZ in our model is a relatively thin rim of tissue made of about 30 to 60 cell layers (sometimes much less) (Figure 1), with tissue beneath the EBZ made essentially of nonviable scar tissue. As the result, the EBZ remains relatively immune to interference by transmurally conducted wave fronts, validating the interpretation of the EBZ maps.

Conclusions

We conclude that there is increased incidence of wave break during VF in the EBZ of hearts with healed MI. The mechanism of increased vulnerability to wave break is compatible with the APD restitution hypothesis.

Acknowledgments

This study was supported in part by Fukuda Memorial Foundation For Medical Technology; National Institutes of Health SCOR grant HL-52319; UC Tobacco-Related Disease Research Program (9RT-0041); American Heart Association National Center grant-in-aid 9750623N and 9956464N; the Cedars-Sinai ECHO Foundation and Grand Sweepstakes; and the Pauline and Harold Price Endowment. We thank Avile McCullen, Mailing Yuan, Babak Armin, and Mariya Favelyukis for technical assistance; Elaine Lebowitz and Nina Wang for secretarial assistance; Drs James N. Weiss and Alan Garfinkel for useful discussions; and Drs P.K. Shah and Teruo Takano for their support.

References

1. Lee JJ, Kamjoo K, Hough D, et al. Reentrant wave fronts in Wiggers' stage II ventricular fibrillation: characteristics and mechanisms of termination and spontaneous regeneration. *Circ Res*. 1996;78:660–675.
2. Mandapati R, Asano Y, Baxter WT, et al. Quantification of effects of global ischemia on dynamics of ventricular fibrillation in isolated rabbit heart. *Circulation*. 1998;98:1688–1696.
3. Kim Y-H, Garfinkel A, Ikeda T, et al. Spatiotemporal complexity of ventricular fibrillation revealed by tissue mass reduction in isolated swine right ventricle: further evidence for the quasiperiodic route to chaos hypothesis. *J Clin Invest*. 1997;100:2486–2500.
4. Zaitsev AV, Berenfeld O, Mironov SF, et al. Distribution of excitation frequencies on the epicardial and endocardial surfaces of fibrillating ventricular wall of the sheep heart. *Circ Res*. 2000;86:408–417.
5. Karma A. Electrical alternans and spiral wave breakup in cardiac tissue. *Chaos*. 1994;4:461–472.
6. Qu Z, Weiss JN, Garfinkel A. Cardiac electrical restitution properties and stability of reentrant spiral waves: a simulation study. *Am J Physiol*. 1999;276:H269–H283.

7. Yashima M, Ohara T, Cao J-M, et al. Nicotine increases ventricular vulnerability to fibrillation in hearts with healed myocardial infarction. *Am J Physiol Heart Circ Physiol.* 2000;278:H2124–H2133.
8. Peters NS, Wit AL. Myocardial architecture and ventricular arrhythmogenesis. *Circulation*. 1998;97:1746–1754.
9. Luke RA, Saffitz JE. Remodeling of ventricular conduction pathways in healed canine infarct border zones. *J Clin Invest.* 1991;87:1594–1602.
10. Matsushita T, Oyamada M, Fujimoto K, et al. Remodeling of cell-cell and cell-extracellular matrix interactions at the border zone of rat myocardial infarcts. *Circ Res*. 1999;85:1046–1055.
11. Uchida T, Yashima M, Gotoh M, et al. Mechanism of acceleration of functional reentry in the ventricle: effects of ATP-sensitive potassium channel opener. *Circulation*. 1999;99:704–712.
12. Kim Y-H, Yashima M, Wu T-J, et al. Mechanism of procainamide-induced prevention of spontaneous wave break during ventricular fibrillation: insight into the maintenance of fibrillation wave fronts. *Circulation*. 1999;100:666–674.
13. Pu J, Boyden PA. Alterations of Na^+ currents in myocytes from epicardial border zone of the infarcted heart: a possible ionic mechanism for reduced excitability and postrepolarization refractoriness. *Circ Res.* 1997;81:110–119.
14. Kadish A, Balke CW, Levine JF, et al. Activation patterns in healed experimental myocardial infarction. *Circ Res*. 1989;65:1698–1709.
15. Karagueuzian HS, Fenoglio JJ, Weiss MB Jr, et al. Protracted ventricular tachycardia induced by premature stimulation of the canine heart after coronary artery occlusion and reperfusion. *Circ Res*. 1979; 44:833–846.
16. Kwan YY, Fan W, Kamjoo K, et al. The effects of procainamide on the characteristics of functional reentry in canine ventricular fibrillation. *Circulation*. 1998;97:1828–1836.
17. Cao J-M, Chen LS, Kenknight BH, et al. Nerve sprouting and sudden cardiac death. *Circ Res*. 2000;86:816–821.
18. Koller ML, Riccio ML, Gilmour RF Jr. Dynamic restitution of action potential duration during electrical alternans and ventricular fibrillation. *Am J Physiol*. 1998;275:H1635–H1642.
19. Cao J-M, Qu Z, Kim Y-H, et al. Spatiotemporal heterogeneity in the induction of ventricular fibrillation by rapid pacing: importance of cardiac restitution properties. *Circ Res*. 1999;84:1318–1331.
20. Ikeda T, Yashima M, Uchida T, et al. Attachment of meandering reentrant wave fronts to anatomic obstacles in the atrium: role of the obstacle size. *Circ Res*. 1997;81:753–764.
21. Kim Y-H, Xie F, Yashima M, et al. Role of papillary muscle in the generation and maintenance of reentry during ventricular tachycardia and fibrillation in isolated swine right ventricle. *Circulation*. 1999;100: 1450–1459.
22. Ikeda T, Wu T-J, Uchida T, et al. Meandering and unstable reentrant wave fronts induced by acetylcholine in isolated canine right atrium. *Am J Physiol*. 1997;273:H356–H370.
23. Pincus SM, Gladstone IM, Ehrenkranz RA. A regularity statistic for medical data analysis. *J Clin Monit*. 1991;7:335–345.
24. Robinson G, Ellis IO, MacLennan KA. Immunocytochemistry. In: Bancroft JD, Stevens A, eds: *Theory and Practice of Histological Techniques*. Edinburg/London/Melbourne/New York: Churchill-Livingstone; 1990:413–436.
25. Karagueuzian HS, Ohta M, Drury KJ Jr, et al. Coronary venous reperfusion of procainamide: a new approach for the management of spontaneous and inducible sustained ventricular tachycardia during myocardial infarction. *J Am Coll Cardiol*. 1986;7:551–563.
26. Friedman P. *GB-Stat*. Silver Spring, Md: Dynamic Microsystems, Inc; 1995.